JOURNAL OF GEOPHYSICAL RESEARCH, VOL. ???, NO. , PAGES 1–25,

Three Dimensional Coronal Density Structure: Paper 1 – Model

S. E. Gibson,[1] D. J. Foster,[2,1] M. Guhathakurta,[3] T. Holzer,[1] and O. C. St. Cyr,[4,5]

[1]High Altitude Observatory, National Center for Atmospheric Research, Boulder, Colorado, USA.

[2]Physics Department, University of Colorado, Boulder, Colorado, USA.

[3]NASA Headquarters, Washington DC, USA.

[4]NASA/GSFC, Greenbelt, MD, USA.

[5]Department of Physics, The Catholic University, Washington, D. C.

Abstract. The three-dimensional density structure of the solar corona is a fundamental boundary condition on the solar wind. Most easily applied models of the global coronal density have been restricted to date to axisymmetric 2D cases. We present here a 3D model made up of a superposition of multiple streamers, having distinct gaussian widths in longitude and latitude and both longitudinal and latitudinal dependence of the neutral lines implicit beneath the streamer cores. Nonradiality of streamers and solar B-angle tilt are also explicitly treated. We show how this simple model can capture many of the general properties of coronal white light observations, and demonstrate how such a model can assist in the interpretation of the multiple views on coronal structures such as will be provided by the upcoming STEREO mission.

1. Introduction

A quantitative description of the 3D, global coronal density is essential to a range of applications. First of all, it represents an important constraint on magnetohydrodynamic (MHD) models of the solar wind and heliosphere (*Sittler and Guhathakurta, 1999; Odstrcil, 2002*). Secondly, despite the dominance of magnetic forces in most of the corona, recent studies show that plasma beta in the core of coronal streamers can be order unity or greater, implying the importance of an accurate determination of large-scale plasma properties for understanding coronal force balance (*Li et al., 1998; Alexander, 1999; Gibson et al.,1999*). Thirdly, quantitative densities determined from coronal white light can be used to eliminate one of the unknowns from observations that depend both on density and other physical parameters (e.g. coronal emission, Faraday rotation). Finally, a realistic model of global coronal density can be very useful as a "toy" model, for example as a background through which to propagate a model coronal mass ejection (CME), or as a forward model to test observational inversion techniques. All of these applications require a model that can reproduce realistic quantitative densities. Moreover, because the corona is in general not axisymmetric, a truly three-dimensional model is to be preferred.

Quantitative coronal density models to date, both 2D and 3D, have ranged from magnostatic or MHD models which define density structures in the context of coronal force balance (e.g. *Bogdan and Low, 1986; Gibson, Bagenal and Low, 1996; Linker et al., 1999; Sittler and Guhathakurta, 1999; Sittler et al., 2003*), to generalized density deconstruction techniques such as tomography that make few assumptions about the nature of coronal density structures, and none about physical force balance (*Frazin and Janzen, 2002; Panasyuk, 1999*). Our work in this paper represents a practical, empirical alter-

native to these, where assumptions are made about the basic sorts of coronal structures to use as building blocks (e.g. coronal holes and streamers). Work of this sort for an essentially axisymmetric corona was done by Guhathakurta *et al.* (1996), demonstrating how the basic shape of a warped streamer belt could be recreated by aligning the streamer core density along a heliomagnetic "equator" rather than the solar rotation axis.

We now expand this type of model into a fully 3D model with the capacity to capture a range of coronal configurations. The benefit of such an *ad hoc* model is its flexibility. Physical models to date have had difficulty extending to three dimensions (see e.g. *Gibson and Bagenal, 1995*), or for fully three-dimensional MHD models, difficulties attaining accurate quantitative density values to match observations (see e.g. discussion in *Gibson et al., 1999*). Tomographic methods require multiple lines of sight to construct density structures: solar rotation can be used under the assumption of minimal evolution, and the three simultaneous views available during the upcoming STEREO mission will greatly improve such methods. However, deconstructions of observations using tomography will continue to be limited to fairly coarse resolution in the azimuthal direction (*Frazin and Janzen, 2002*). The model described in this paper can be used to simulate the density of a realistic, three-dimensional corona with as great a degree of complexity as is desired. Moreover, such models are easily reproducible given the set of parameters that defines them, making them eminently portable to a range of applications – such as testing the sensitivity of tomographic methods to the presence of structures of varying size scales and orientations. This model can also be used to quantitatively determine a global coronal density distribution directly from observations (which also necessitate assumptions about

minimal time evolution): this will be the subject of a companion paper on model fitting techniques (*Gibson et al., 2003*).

In section 2 we will discuss observations of coronal streamers, both in their historical context, and also specifically the data that we will use in this and in our companion paper. In section 3 we will describe the model of Guhathakurta *et al.* (1996) upon which our expanded model is based, and discuss axisymmetric modifications of it. In section 4 we will expand the model to fully three dimensions, and show how the variety of coronal observed features increases with the various modifications. In section 5 we will briefly discuss how observations from the upcoming STEREO will assist in applying this model, and in section 6 we will present our conclusions.

2. Background: coronal streamer observations

Figure 1 shows a solar eclipse image of the corona in white light. The light is largely emitted at the photosphere but is scattered off of coronal electrons, so the observable is proportional to electron density (*Billings, 1966*). From this figure we see that there are regions of enhanced density concentrated towards the solar equator, and regions of depleted density at the solar poles: the standard configuration near solar minimum. The enhanced regions are commonly called helmet streamers. These helmet streamer regions roughly correspond to large, closed loop magnetic structures when compared to extrapolations of the photospheric magnetic field: physically therefore they may be taken to represent coronal plasma trapped by large-scale closed magnetic field. Helmet streamers have been modeled as a fundamental building block of the corona for decades (see Guhathakurta *et al.,* (1996), and references therein).

Because the observed brightness arises from an integral of the density along the line of sight, it is generally true that the three-dimensional form of coronal plasma needs to be considered in extracting density from the white light images. Since the sun rotates, some information on this three-dimensional structure can be found by looking at entire solar rotations of white light (assuming minimal evolution of structures). Figure 2 shows an example of data from just over one solar rotation at solar minimum: observations of the white light corona as a function of latitude vs. longitude for a given height (known as a Carrington map). Helmet streamers here appear as mainly horizontal structures: for greater heights they become more and more grouped towards the equator. For this reason many have used the first-order approximation of helmet streamers as an axisymmetric structure, or belt, around the equator. Guhathakurta *et al.* (1996) took this one step further and, using observations for a series of rotations near solar minimum, found that such a belt was more accurately fit when centered around a tilted heliomagnetic equator. They also found the distribution in latitude was well-fit by a Gaussian profile, when centered on the tilted heliomagnetic equator.

In this paper, we will present a model that is truly three-dimensional, and so we are interested in a time period when coronal helmet streamers are less axisymmetric. Figure 3 shows such a time period, with streamers appearing as structures with varying widths in latitude and lengths in longitude. Figures 3a-b have significant data dropouts (vertical black bands): these arise because of bad weather at the (ground-based) Mauna Loa Observatory where these lower heights were observed. Until we have space-based observations of the lower corona (such as those planned for the STEREO mission discussed in section 5), we cannot avoid weather. Although Carrington rotations exist with greater ground-

based coverage, we chose this time period because it represented a period far enough from solar minimum for non-axisymmetric streamers to be common, yet not so close to solar maximum that streamer complexity and time variation made it pointless to fit with a parameterized, static model such as ours. Our choices of time interval were further reduced by the availability of SOHO/LASCO data: the rotation of Figure 3 occurred between two extended data dropouts for SOHO/LASCO. Finally, we chose this rotation because it lay near the time of the Spartan 201-05 mission, which, during the 40 hours of its observations, yielded unprecedented coverage vs. radius of the white light corona. Data from the Spartan mission time are shown in Figure 4 c, and are used in the axisymmetric fit to data described in the companion paper to this one (Gibson *et al.*, 2003).

3. Axisymmetric model

3.1. Model of Guhathakurta *et al.* (1996)

We have already described how at solar minimum helmet streamers are concentrated about the solar equator, corresponding to material trapped in a basically dipolar magnetic field, symmetric about the axis of solar rotation. As the sun evolves away from solar minimum, but is still far from solar maximum, the large-scale magnetic field can be approximated as a dipole that is tilted by some angle to the solar rotation axis. The helmet streamer belt then is centered about the plane of its own tilted heliomagnetic equator. The solar wind opens up the magnetic field into a more and more radial configuration with increasing height, concentrating the streamer belt into a thin current sheet. Solar rotation ultimately extends the magnetic field into an Archimedian spiral, where the warped current sheet separates the magnetic field into two heliomagnetic sectors of opposing polarity.

This picture of a tilted dipole is a fairly commonly accepted description of the near-solar minimum magnetic field, and one which Guhathakurta *et al.,* (1996) used as physical motivation for an empirical model where coronal density is allowed variation in both heliographic latitude and longitude (θ and ϕ). This angular variation is implicit in the equation describing the angular separation (i.e. heliomagnetic latitude, θ_{mg}) between a coronal source at heliographic coordinates (r, θ, ϕ) and the heliomagnetic equator (or core neutral line) of a tilted dipole, i.e.:

$$\theta_{mg} = sin^{-1}[-cos\theta sin\alpha_1 sin(\phi - \phi_o) + sin\theta cos\alpha_1], \quad (1)$$

Here α_1 is the tilt angle of the magnetic dipole equator with respect to the heliographic equator, and ϕ_o is the longitude of the intersection of the heliomagnetic and heliographic equators.

Guhathakurta *et al.,* (1996) determined the parameters α_1 and ϕ_o from observations of white light for several rotations near solar minimum (an alternative technique would be to define the location of the magnetic latitude using extrapolations of observed photospheric magnetic field: see discussion and references in Guhathakurta *et al.,* (1996)). When the white light data were organized about this central heliomagnetic latitude, the data followed a basically Gaussian distribution about it. The widths of these Gaussian distributions decreased with radial height, due to the solar wind expansion of open field in the polar coronal holes which simultaneously contracts the streamers towards a central current sheet. For these physical and observational reasons, the authors chose the following empirical form for coronal density:

$$N(r, \theta_{mg}) = N_p(r) + [N_{sc}(r) - N_p(r)]e^{-\theta_{mg}^2/w^2(r)} \quad (2)$$

Here $N(r, \theta_{mg})$ is the electron number density per cm^3, $N_{sc}(r)$ and $N_p(r)$ are the radial profiles of electron density along the streamer core and polar coronal hole respectively, and $w(r)$ is the $1/e$ width of the streamer (fit to a radial polynomial function). Using radial density profiles determined from fits to brightness at the pole and heliomagnetic equator, the authors showed that upon integration along the line of sight, the model reproduced coronal brightnesses well in the time periods they considered (near solar minimum).

This model is an effective means to capture the properties of the tilted dipole, in particular for time periods such as the declining phase of the solar cycle when such a modeled configuration matches observations well. However, closer to solar maximum, a single tilted-dipole streamer belt becomes a less accurate model. Moreover, although density varies with the three heliographic coordinates, it is symmetric about the heliomagnetic equator. Fully three dimensional variations, such as sub-structures in the streamer belt (i.e. multiple streamers visible at lower coronal heights which merge into something closer to a single current sheet at larger heights) are not allowed.

3.2. Axisymmetric modifications to model

We can immediately adapt the model in two ways, without losing axisymmetry: that is, by allowing multiple streamer belts, and by allowing the non-radial deflection of streamers. For simplicity, in this section we will not consider tilted streamer core neutral lines, but rather treat a system that is truly axisymmetric about the rotation axis. We will return

to more complete angular variations of θ_{mg} in Section 4, when we consider the full three-dimensional model.

3.2.1. Multiple streamer belts.

We allow for multiple streamer belts by expanding Equation 1 to become:

$$N(r,\theta) = N_p(r) + \Sigma_i \Big[[N_{sc_i}(r) - N_p(r)] e^{-\theta^2_{mg_i}/w_i^2(r)} \Big] \tag{3}$$

Here the subscript i represents each streamer belt to be included in the model. Each streamer belt will have its own core profile $N_{sc_i}(r)$, its own central core θ_{o_i} (so that $\theta_{mg_i} = \theta - \theta_{o_i}$), and its own width $w_i(r)$. Note we define the widths to be:

$$\begin{aligned} w_i(r) &= a_i + b_i * r && (r < R_{cs_i}) \\ w_i(r) &= a_i + b_i * R_{cs_i} && (r > R_{cs_i}) \end{aligned} \tag{4}$$

Since the width of the streamer decreases with height, b_i will be negative. In order to avoid negative widths at large heights, we ensure that the width goes to a constant at a specified height R_{cs_i} before that can occur.

We also define the core (N_{sc}) and polar hole (N_p) radial density profiles (following Sittler and Guhathakurta (1999)):

$$N_p(r) = A_o e^{(A_1/r + A_2/r^2)}(1 + A_3/r + A_4/r^2 + A_5/r^3)/r^2 \tag{5}$$

$$N_{sc_i}(r) - N_p(r) = B_{o_i} e^{(B_{1_i}/r + B_{2_i}/r^2)}(1 + B_{3_i}/r + B_{4_i}/r^2 + B_{5_i}/r^3)/r^2 \tag{6}$$

The first exponential term in these expansions models an isothermal hydrostatic atmosphere, but is modified by the second exponential term which simulates the effect of a decreasing temperature gradient. These terms dominate in the lower corona (small r). At very large r, the profiles go to a $1/r^2$ profile as the solar wind expansion dominates. In between, the polynomial terms allow a general fit to observations. We express the

difference $N_{sc_i}(r) - N_p(r)$ in terms of the positive definite polynomial in order to ensure that the streamer core density profile is always greater than the coronal hole profile so that streamers always add density to the background, and never remove density.

3.2.2. Nonradial streamers.

Observations often show that streamers at high latitude do not project outward radially, but rather are deflected towards the solar equator (e.g. Figure 4c – compare the NE streamer to the radial line drawn). In order to model this, we center each streamer along a core neutral line (θ_{nl_i}) which originates along a latitude θ_{o_i} at the coronal base and extends outwards at an angle α_{2_i} to the radial,

$$\theta_{nl_i}(r) = \theta_{o_i} + \Big[\alpha_{2_i} - sin^{-1}[\frac{sin\alpha_{2_i}}{r}]\Big] \tag{7}$$

The heliomagnetic latitude from any point (r, θ, ϕ) to this neutral line is then $\theta_{mg_i} = \theta - \theta_{nl_i}(r)$. The tilted radial coordinate that the streamers are oriented along is:

$$r'_i = 1 - cos\alpha_{2_i} + \sqrt{r^2 - sin^2\alpha_{2_i}} \tag{8}$$

Using the revised heliomagnetic latitude, and the transformed radial coordinate for the streamers, Equation 3 then becomes

$$N(r,\theta) = N_p(r) + \Sigma_i\Big[[N_{sc_i}(r'_i) - N_p(r)]e^{-\theta^2_{mg_i}/w^2_i(r'_i)}\Big] \tag{9}$$

Figures 4a and b show an example of a modeled three-streamer belt axisymmetric configuration, with both the northern and southern streamers deflected nonradially towards the equator. Figure 4c shows a similar configuration observed during the Spartan 201-05 mission. Note that details of the actual fit to data are discussed in the companion paper to this one (*Gibson et al., 2003*).

4. 3D extension of model

4.1. Finite longitudinal streamers

Figure 3 shows a Carrington map for a solar rotation occurring soon after the single day's image shown in Figure 4c. The finite longitudinal lengths of streamers in these observations demonstrate the three-dimensionality of the corona. Although some of the variations of brightness with longitude can be explained by projection effects acting on a streamer belt that encircles the sun (see *Guhathakurta et al., 1996* and *Wang, 1997* for discussion), not all of them can, particularly in the lower corona. Therefore we would like to have the option of including streamers of finite longitudinal extent in our model.

4.1.1. Modification of model to include finite streamers.

We include variation of streamers with longitude as follows:

$$N(r,\theta,\phi) = N_p(r) + \Sigma_i \Big[[N_{sc_i}(r'_i) - N_p(r)] e^{-\theta^2_{mg_i}/w_i^2(r'_i)} e^{-\phi^2_{mg_i}/v_i^2(r'_i)} \Big] \qquad (10)$$

Thus we have allowed a Gaussian variation versus longitude as well as that versus latitude. The magnetic longitude is $\phi_{mg_i} = \phi - \phi_{o_i}$ for each streamer, where ϕ_{o_i} is the central longitude for each streamer core (note that the periodic coordinate ϕ should be chosen such that ϕ_{mg_i} lies in the domain $(-\pi, \pi)$, in order that Equation 10 is continuous everywhere). We define the gaussian width in longitude, $v_i(r'_i)$, as directly proportional to the gaussian width in latitude, implying streamers with elliptical cross-sections. (An alternative approach was suggested by Mancuso and Spangler (2000), who altered the basic Guhathakurta *et al.* (1996) model by allowing the latitudinal width w to vary with both r and ϕ.) For the time period of Figure 3, the horizontal, or longitudinal ellipse axis is generally the longer one, presumably because solar wind expansion is greatest in the polar holes, and so the streamers are most contracted in latitude.

4.1.2. Effect of finite streamers on observable structures.

Figure 5 shows examples of modeled finite streamers as a function of latitude vs. longitude for three heights, both for density, and integrated white light. Four streamers have been included in this model: the first one in the northern hemisphere (centered at 100° longitude) is a relatively squat, radial streamer. Two other, wider and more nonradial streamers can be seen in the southern hemisphere (centered at 80° and 240° longitude). Note that the southern streamer to the right does not extend as far out radially as the southern streamer to the left, and has nearly disappeared by a height of $r = 2.5R_{sun}$. Finally, we have included an equatorial streamer that is nearly axisymmetric. By $r = 2.5R_{sun}$ this streamer has more or less merged with the two southern streamers, which tilt equatorward to join with it in what appears as a single current sheet.

One of the most useful aspects of a simple parameterized model such as ours is that we can intuitively see the consequences of line of sight integration as well as measure it quantitatively. The observable, polarized brightness, or pB, is proportional to the integral along the line of sight of the coronal electron density. This integration leads to significant differences in the appearance of density as opposed to pB structures in the latitude vs. longitude maps. One nice example is the "banana"-shape that the northern streamer takes on when seen in integrated pB. The reason for the existence of these shapes is that when a streamer is not centered on the limb of the sun, and is tilted at an angle to the ecliptic plane (as for example radial streamers are away from the equator), its projection along the line-of-sight onto the limb can yield a streamer center at a (for radial streamers) higher latitude. For the northern streamer in Figure 5, the projection effect is identical when the streamer is in front or behind the limb, leading to a symmetric banana shape in

the pB Carrington maps (indicated by the white arrows), as the center of the projected pB streamer moves from higher latitudes, to lower latitudes, and back to higher latitudes.

Are these bananas observed? Certainly: the white arrows in Figure 3c demonstrate this. The effect is somewhat diminished by the polar solar wind's natural tendancy to push higher latitude streamers towards the ecliptic plane, i.e. the nonradial tilt of the streamers that our model explicitly treats. This is why the southern streamers in our model do not have obvious banana shapes in pB, as we have imposed greater nonradiality towards the equator on them than on the northern streamer. Also note that this banana effect requires streamers having finite width in longitude: it is an effect that would not occur in the same manner for a continuous streamer belt encircling the Sun as in the original Guhathakurta *et al.* (1996) model.

4.2. Variation of θ_{mg_i} with latitude and longitude

We have so far dealt with streamers that, for a given height, lie along a constant latitude. As in the original Guhathakurta *et al.* (1996) model, we can also allow the orientation of the streamers' core neutral lines to depend upon longitude. Rather than fit a single current sheet function to observations as was done in that paper, we allow each streamer to be centered above an angled neutral line. The more complex, warped current sheet apparent at large heights can still be retrieved as a superposition of angled streamers, without losing the sub-structures of more individuated streamers.

4.2.1. Modification of model to allow angled neutral lines.

The heliomagnetic latitude is basically the shortest distance from a point (r, θ, ϕ) to each streamer's core neutral line along the sphere of radius r. Up till now those core neutral lines ($\theta_{nl_i}(r)$) have not varied with ϕ, so that $\theta_{mg_i} = \theta - \theta_{nl_i}(r)$. In order to

achieve streamers aligned along neutral lines that are tilted with a slope m_i with respect to longitude (and which still are allowed to be nonradial), we now define the neutral lines by:

$$\theta_{nl_i}(r,\phi) = \theta_{o_i} + m_i(\phi - \phi_{o_i}) + \Big[\alpha_{2_i} - sin^{-1}[\frac{sin\alpha_{2_i}}{r}]\Big] \tag{11}$$

The heliomagnetic latitude is no longer simply $\theta - \theta_{nl_i}$, as this is no longer the minimum distance to the neutral line. Instead it is the projection:

$$\theta_{mg_i}(r,\theta,\phi) = (\theta - \theta_{nl_i})/(1 + {m_i}^2)^{\frac{1}{2}} \tag{12}$$

The heliomagnetic longitude, as described above, is the distance between ϕ and ϕ_{o_i} – but it is the distance along the neutral line, which now becomes:

$$\phi_{mg_i}(r,\theta,\phi) = m_i\theta_{mg_i} + (1 + {m_i}^2)^{\frac{1}{2}}(\phi - \phi_{o_i}) \tag{13}$$

Finally, because our tilted Gaussian profiles are intrinsically discontinuous at the periodic ϕ boundaries, we truncate the Gaussian at its greatest value along the $\phi - \phi_{o_i} = \pm\pi$ boundaries. This is done by subtracting this maximum value everywhere within the truncated Gaussian, and setting the streamer function equal to zero everywhere outside of it. This ensures that the contribution from the tilted streamers are identically zero at the the $\phi - \phi_{o_i} = \pm\pi$ boundaries, and so removes the discontinuity.

Thus Equation 10 becomes:

$$N(r,\theta,\phi) = N_p(r) + \Sigma_i\Big[[N_{sc_i}(r'_i) - N_p(r)]F_{gauss_i}(r'_i,\theta_{mg_i},\phi_{mg_i})\Big] \tag{14}$$

where $F_{gauss_i} = e^{-\theta^2_{mg_i}/w_i^2(r'_i)}e^{-\phi^2_{mg_i}/v_i^2(r'_i)} - F_{trunc_i}(r'_i)$ if $e^{-\theta^2_{mg_i}/w_i^2(r'_i)}e^{-\phi^2_{mg_i}/v_i^2(r'_i)} > F_{trunc_i}(r'_i)$

and $F_{gauss_i} = 0$ if $e^{-\theta^2_{mg_i}/w_i^2(r'_i)}e^{-\phi^2_{mg_i}/v_i^2(r'_i)} < F_{trunc_i}(r'_i)$

$F_{trunc_i}(r'_i)$ can be found by solving for the maximum of the Gaussian along $\phi - \phi_{o_i} = \pm\pi$, i.e.:

$$F_{trunc_i}(r'_i) = e^{-\theta^2_{max_i}/w_i^2(r'_i)} e^{-\phi^2_{max_i}/v_i^2(r'_i)}$$

$$\theta_{max_i} = \frac{-m_i({m_i}^2+1)^{\frac{1}{2}} w_i^2}{v_i^2 + m_i^2 w_i^2}\pi$$

$$\phi_{max_i} = m_i\theta_{max_i} + (1+m_i^2)^{\frac{1}{2}}\pi$$

4.2.2. Effect of angled neutral lines on observable structures.

Figure 6 shows examples of streamers with angled underlying neutral lines. They are the same four streamers as shown in Figure 5, except that each has some degree of $\theta - \phi$ slope. This leads to an increased warping of the central current sheet. Another change is that the northern bananas are no longer symmetric: because of the angle of the underlying neutral line, one side of the banana is enhanced, leading to an asymmetric banana.

4.3. Solar B angle

One final modification is to include the effects of the tilt of the Sun-Earth line of sight that occurs semi-annually due to the difference between the Earth's plane of rotation and the Sun's axis of rotation over the course of the Earth's orbit around the Sun. This is known as the solar B angle, and moves from a maximum of 7.25° (North) in early September, to a minimum of −7.25° (South) in early March. Since this angle is a purely line-of-sight effect, it does not affect our density model. However it does affect the pB that would be observed. Figure 7 shows plots of pB for the same density model as that shown in Figure 6, except integrated along a line of sight for the case of maximum B angle. This line of sight introduces an obvious East-West asymmetry: the left-hand figures (a-c) are Carrington maps made up of observations taken at the East limb, and the right-hand

figures (d-f) are made up of observations taken at the West limb. (Note that in Figures 3, 5, and 6, where the B-angle is zero, East limb and West limb maps were identical.) A general effect of observing from 7.25° North is to slant West limb projected structures further up and to the left (or equivalently down and to the right), and to slant East limb projected structures further up and to the right (or equivalently down and to the left). (See Li *et al.* (2000), for a similar effect found for observed and modeled "polar rays")

Figure 3 showed observations taken in November, when the B angle was nearly zero. Thus we would not expect to observe East-West asymmetries of the nature described above in those data. However, Figure 2 shows observations taken during a time of maximal B angle (September 1996), which indeed shows a pronounced East-West asymmetry in Carrington maps. Of course the nature of solar limb synoptic maps is such that we cannot be sure that such an asymmetry is not in part due to evolution of structures, since the observations making up the East and West limb maps are taken two weeks apart for a given longitude. However, the model demonstrates that at least some of the asymmetry can be due to the presence of the solar B angle: indeed, the net trend in the East limb maps of Figure 2 is for structures slanted up and to the right, and in the West limb maps, structures slanted up and to the left, just as it is in our simple model. And for this particular rotation, a lack of solar activity made the conclusion that solar B angle was the main reason for the asymmetry quite plausible (see Wang (1997) and Biesecker *et al.* (1999) for further discussion of the effect of solar B angle on this rotation).

4.4. Equations

For clarity, we now list the equations that make up the full 3-D model:

$$N(r,\theta,\phi) = N_p(r) + \Sigma_i\Big[[N_{sc_i}(r_i') - N_p(r)]F_{gauss_i}(r_i', \theta_{mg_i}, \phi_{mg_i})\Big]$$

$$N_p(r) = A_o e^{(A_1/r + A_2/r^2)}(1 + A_3/r + A_4/r^2 + A_5/r^3)/r^2$$

$$N_{sc_i}(r_i') - N_p(r) = B_{o_i} e^{(B_{1_i}/r_i' + B_{2_i}/r_i'^2)}(1 + B_{3_i}/r_i' + B_{4_i}/r_i'^2 + B_{5_i}/r_i'^3))/r_i'^2$$

$$r_i' = 1 - cos\alpha_{2_i} + \sqrt{r^2 - sin^2\alpha_{2_i}}$$

$$\theta_{mg_i} = (\theta - \theta_{nl_i})/(1+m^2)^{\frac{1}{2}}$$

$$\theta_{nl_i}(r,\phi) = \theta_{o_i} + m_i(\phi - \phi_{o_i}) + \Big[\alpha_{2_i} - sin^{-1}[\frac{sin\alpha_{2_i}}{r}]\Big]$$

$$\phi_{mg_i} = m\theta_{mg_i} + (1+m^2)^{\frac{1}{2}}(\phi - \phi_{o_i})$$

$$F_{gauss_i} = e^{-\theta_{mg_i}^2/w_i^2(r_i')}e^{-\phi_{mg_i}^2/v_i^2(r_i')} - F_{trunc_i}(r_i') \text{ if } e^{-\theta_{mg_i}^2/w_i^2(r_i')}e^{-\phi_{mg_i}^2/v_i^2(r_i')} > F_{trunc_i}(r_i')$$

$$F_{gauss_i} = 0 \text{ if } e^{-\theta_{mg_i}^2/w_i^2(r_i')}e^{-\phi_{mg_i}^2/v_i^2(r_i')} < F_{trunc_i}(r_i')$$

$$F_{trunc_i}(r_i') = e^{-\theta_{max_i}^2/w_i^2(r_i')}e^{-\phi_{max_i}^2/v_i^2(r_i')}$$

$$\theta_{max_i} = \frac{-m_i({m_i}^2+1)^{\frac{1}{2}}w_i^2}{v_i^2 + m_i^2 w_i^2}\pi$$

$$\phi_{max_i} = m_i\theta_{max_i} + (1+m_i^2)^{\frac{1}{2}}\pi$$

$$w_i(r_i') = a_i + b_i * r_i' \qquad (r' < R_{cs_i})$$

$$w_i(r_i') = a_i + b_i * R_{cs}; \qquad (r' > R_{cs_i}))$$

$$v_i(r_i') = c_i * w_i(r_i')$$

Here (r,θ,ϕ) are the heliographic coordinates, $N(r,\theta,\phi)$ is the electron density, $N_p(r)$ is the polar density radial profile, and $N_{sc_i}(r_i')$ are the streamer core profiles which vary along r_i', the transformed radial coordinate that lie at angles α_{2_i} with respect to r. The streamers are concentrated in a truncated Gaussian profile F_{gauss_i} about the core neutral lines that

are defined by the θ_{nl_i}. The minimum distance from a heliographic position (r, θ, ϕ) to the neutral line (along the sphere of radius r) define the heliomagnetic latitudes θ_{mg_i}, and the distance along the neutral line to the streamer core is the heliomagnetic longitude ϕ_{mg_i}. The Gaussian width with respect to latitude is w_i, and with respect to longitude is v_i, and R_{sc_i} is the height above which the current sheets have constant thickness. The Gaussian is truncated along the $\phi - \phi_{o_i} = \pm\pi$ boundary by subtracting the maximum value at this boundary at $(\theta_{max_i}, \phi_{max_i})$.

5. Applications for the STEREO mission

The STEREO mission, due to launch in late 2005, will have two spaceship launched such that one will move ahead of the Earth in its orbit, and the other lag behind. Thus, with the inclusion of coronagraphs that lie along the Earth's line of sight, there will be three sets of coronagraphs observing the Sun from three different viewing angles. This will greatly aid in resolving some of the issues of interpreting and fitting observed coronal data. There will probably be several standard formats for STEREO data: Carrington maps are likely to be one. Therefore we now will consider how Carrington maps, in conjunction with our model, could address the issues of time variation and model degeneracy. In particular, we will consider how the effect of solar B angle variation combines with time variation of structures to change the appearance of structures from different viewpoints.

First of all, we consider the rather critical issue of time evolution. Carrington maps implicitly assume no significant evolution of structures over the course of the solar rotation. This is not a good assumption, particularly at solar maximum. STEREO will permit three angles viewed simultaneously. If there were no variation in solar B angle between the spacecraft, the structures viewed by the lagging STEREO coronagraph could be compared

to those viewed at the same heliographic longitude by the other two coronagraphs as solar rotation brought the structures past some time later, and any difference would be due to time evolution. Moreover, a total of six views (East and West limb for each of the three viewing angles) could provide six simultaneously observed longitudes that could be combined into a somewhat coarse, but completely co-temporal Carrington map. However, as the spacecraft separate from the Earth, they will generally have different B angles, and such a combined Carrington map may be difficult to interpret directly. There will be important exceptions when two of the three sets of coronagraphs could have identical B angles (that is, when one is approaching a B-angle extrema, and the other is receding from it): such times would be excellent to study the effects of time variation on Carrington maps. More generally, since we have some understanding of how the change in B angle affects structures (i.e. their overall slant is affected as described above), we can attempt to separate B angle effects from those of time evolution when we compare Carrington maps constructed independently from each viewing angle.

The fact that we will have six co-temporal limb observations will, however, be helpful for fitting models such as ours to observations. As we will discuss in the companion paper (*Gibson et al., 2003*), our model can be fit to observations using a genetic algorithm forward technique (*Gibson and Charbonneau, 1998*). Because the B angle of each coronagraph can be explicitly included in the forward model calculation of the pB to be compared to observations, the B angle differences can actually be used to help reduce the degeneracy of possible solutions for a model fit. Even today, for a solar rotation with minimal or no time evolution, occuring during a time of significant B angle, we could use the East and West Carrington maps to double the data a model would have to match (CROT

1912 shown in Figure 2 is a possible example). With STEREO, we could in theory create six distinct sets of Carrington maps that the model would have to simultaneously fit, greatly reducing the degeneracy. Since we do expect significant time evolution in general, however, perhaps the best approach would be to examine the independently constructed Carrington maps for each viewpoint in order to get a feel for the importance of time evolution, and from these establish a confidence level to assign to observations taken at progressively removed times from the portions of each map that were nearly co-temporal. In this manner we could fill in a weighted set of observations to use in model fitting.

6. Conclusions

In summary, we have developed a fully three-dimensional density model which captures much of the complexity of coronal structures observed in white light. This model represents a middle ground between full MHD simulations and tomographic methods: it does not solve for density in the context of coronal force balance, but it is made up of the building blocks of coronal holes and streamers which are based on a physical interpretation of coronal observations. Most importantly it has the flexibility implicit to a parameterized model that will enable its easy application to a range of problems. We foresee such applications to be two-fold: first as a realistic forward "toy" model of significantly greater three-dimensional complexity than has been presented in the past, and second as a method for determining quantitative three-dimensional density models from observations.

The use of the model to fit observations will be discussed in our companion paper, Gibson *et al.* (2003), and has potentially wide applications: for example three-dimensional coronal densities can be used as boundaries on heliospheric models, and also in combi-

nation with other datasets to quantify coronal plasma properties (see e.g. *Mancuso and Spangler, 2000* for an application of a similar but simpler density model to Faraday rotation analysis). Although we believe that MHD models and/or tomographic methods will ultimately be the preferred methods for determining three-dimensional quantitative coronal densities, at present neither method is completely successful. For the present, our *ad hoc* model provides a viable alternative.

The model may well be most useful, however, as a forward toy model. Starting from a quantitatively realistic base configuration (perhaps obtained from a fit to observation), one can examine the effects of varying the size, shape, relative densities, and orientations of streamers on projected white light observations. From this one can gain intuition on what sort of structures actually exist in the corona. Even more practically, one can examine the sensitivity of inversion techniques like tomography to such a variety of structures, and work to improve those techniques. One can also use the global coronal density as a base template for an MHD simulation, and examine how a CME would dynamically interact with such a background. Because it is an easily portable model that anyone can apply, the potential for such exploratory studies is very large.

Acknowledgments. We thank Nick Arge for internal NCAR review of this paper, and Joan Burkepile and Giuliana de Toma for helpful discusssion. S. G., D. F., and O. C. S-C acknowledge NAG-5-8018 subcontract HAO02242, S. G. and T. H. also acknowledge NASA PO S-13797-G. S. G.'s and D. F.'s work is supported in part by CISM which is funded by the STC Program of the National Science Foundation under Agreement Number ATM-0120950. The SOHO/LASCO data used here are produced by a consortium of the Naval Research Laboratory (USA), Max-Planck-Institut fuer Aeronomie (Germany)),

Laboratoire d'Astronomie (France), and the University of Birmingham (UK). SOHO is a project of international cooperation between ESA and NASA.

References

Alexander, D., Temperature structure of the quiet Sun X-ray corona, *J. Geophys. Res.,104,* 9691,1999.

Biesecker, D. A., Thompson, B. J., Gibson, S. E., Alexander, D., Fludra, A., Gopalswamy, N., Hoeksema, J. T., Lecinski, A., and L. Strachan, Synoptic Sun during the first Whole Sun Month Campaign: August 10 to September 8, 1996, *J. Geophys. Res., 104,* 9679, 1999.

Bogdan, T. J., and Low, B. C., The three-dimensional structure of magnetic atmospheres II: Modeling the large-scale corona, *Astrophys. Journ., 306*, 271, 1986.

Billings, D. E., A Guide to the Solar Corona, *New York: Academic*, 1966.

Frazin, R. A., and Jansen, P., Tomography of the solar corona. II. Robust, reularized, positive estimation of the three-dimensional electron density distribution from LASCO-C2 polarized white-light images, *Astrophys. Journ., 570*, 408, 2002.

Gibson, S. E., and Bagenal F., The large scale magnetic field and density distribution in the solar minimum corona, *J. Geophys. Res., 100*, 19,865, 1995.

Gibson, S. E., Bagenal, F., and B. C. Low, Current sheets in the solar minimum corona, *J. Geophys. Res., 101*, 4813, 1996.

Gibson, S. E., and Charbonneau, P., Empirical modeling of the solar corona using genetic algorithms, *J. Geophys. Res., 103*, 14,511, 1998.

Gibson, S. E. , Biesecker, D., Guhathakurta, M., Hoeksema, J. T., Lazarus, A. J., Linker, J., Mikic, Z., Pisanko, Y., Riley, P., Steinberg, J., Strachan, L., Szabo, A., Thompson, B. J., and X. P. Zhao, The three-dimensional coronal magnetic field during Whole Sun Month, *Astrophys. Journ., 520*, 871, 1999.

Gibson, S. E., *et al.*, Three dimensional coronal density structure: Paper 2 – fit to data, *in prepraration*, 2003.

Guhathakurta, M.l, Holzer, T. E., and R. M. MacQueen, The large-scale density structure of the solar corona and the heliospheric current sheet, *Astrophys. Journ., 438*, 817, 1996.

Li, J., Raymond, J. C., Acton, L. W., Kohl, L., Romoli, M., Noci, G., and G. Naletto, Physical structure of a coronal streamer in the closed field region as observed from UVCS/SOHO and SXT/Yohkoh, *Astrophys. Journ., 506*, 438, 1998.

Li, J., Jewitt, D., and B. Labonte, The nature of solar polar rays, *Astrophys. Journ., 539*, L67, 2000.

Linker, J. A., Mikic, Z., Biesecker, D. A., Forsyth, R. J., Gibson, S. E., Lazarus, A. J., Lecinski, A., Riley, P., Szabo, A., and B. J. Thompson, Magnetohydrodynamic modeling of the solar corona during Whole Sun Month, *J. Geophys. Res., 104*, 9809, 1999.

Mancuso, S., and Spangler, S. R., Faraday rotation and models for the plasma structure of the solar corona, *Astrophys. Journ., 539*, 480, 2000.

Odstrcil, D., Linker, J. A., Lionello, R., Mikic, Z., Riley, P., Pizzo, V. J., and J. G. Luhmann, Merging of coronal and heliospheric numerical two-dimensional MHD models, *J. Geophys. Res., 107*, SSH 14-1, CiteID 1493, 2002.

Panasyuk, A., Three-dimensional reconstruction of UV emissivities in the solar corona using Ultraviolet Coronagraph Spectrometer data from the Whole Sun Month, *J. Geo-*

phys. Res., 104, 9721, 1999.

Sittler, E. C., Jr., and M. Guhathakurta, Semiempirical two-dimensional magnetohydrodynamic model of the solar corona and interplanetary medium, *Astrophys. Journ,, 523*, 812, 1999.

Sittler, E. C., Jr., Ofman, L., Gibson, S., Guhathakurta, M., Davila, J., Skoug, R., Fludra, A., and T. Holzer, Development of multidimensional MHD model for the solar corona and solar wind, *Proceeds of Solar Wind 10, in press*, 2003.

Wang, Y.-M., Sheeley, N. R., Jr., Howard, R. A., Kraemer, J. R., Rich, N. B., Andrews, M. D., Brueckner, G. E., Dere, K. P., Koomen, M. J., Korendyke, C. M., Michels, D. J., Moses, J. D., Paswaters, S. E., Socker, D. G., Wang, D., Lamy, P. L., Llebaria, A., Vibert, D., Schwenn, R., and G. M. Simnett, Origin and Evolution of Coronal Streamer Structure during the 1996 Minimum Activity Phase, *Astrophys. Journ., 485*, 875, 1997.

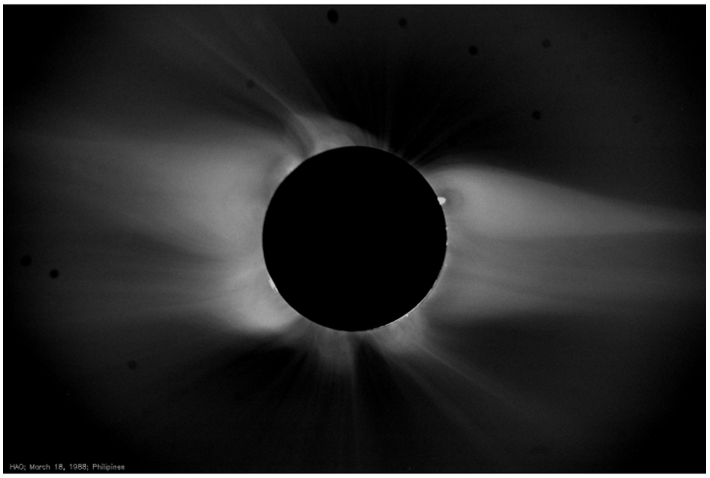

Figure 1. 1988 total solar eclipse image (Phillipines) courtesy High Altitude Observatory (HAO), University Corporation for Atmospheric Research (UCAR), Boulder, Colorado. UCAR is sponsored by the National Science Foundation.)

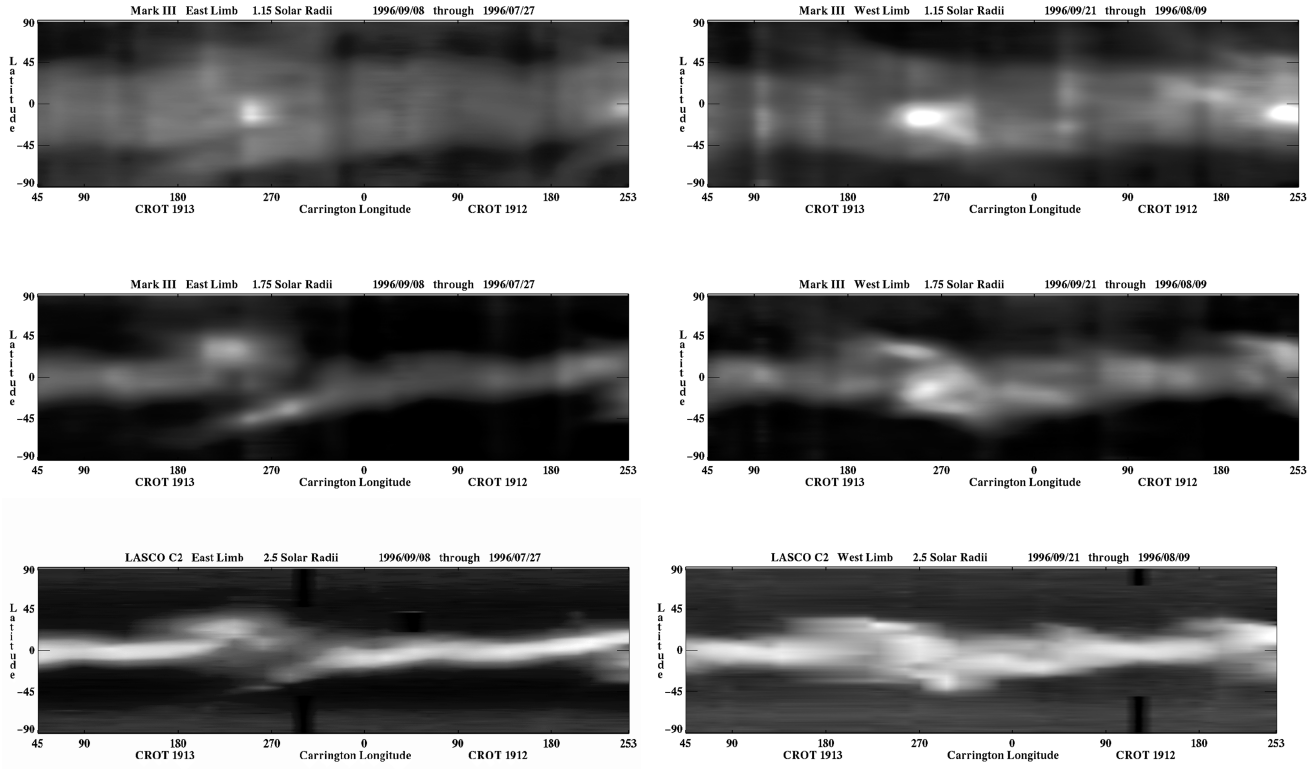

Figure 2. Carrington maps of the six weeks surrounding the Whole Sun Month (August/September 1996 – see Biesecker *et al.* (1999)), showing observations of white light observable (pB) as a function of latitude vs. longitude, for three heights: $r = 1.15R_{sun}$; $r = 1.75R_{sun}$; and $r = 2.5R_{sun}$. Left figures show maps made from images of the East limb, right figures show maps made from the West limb. Data are from the Mauna Loa Mark III K-Coronameter and LASCO C2 Coronagraph.

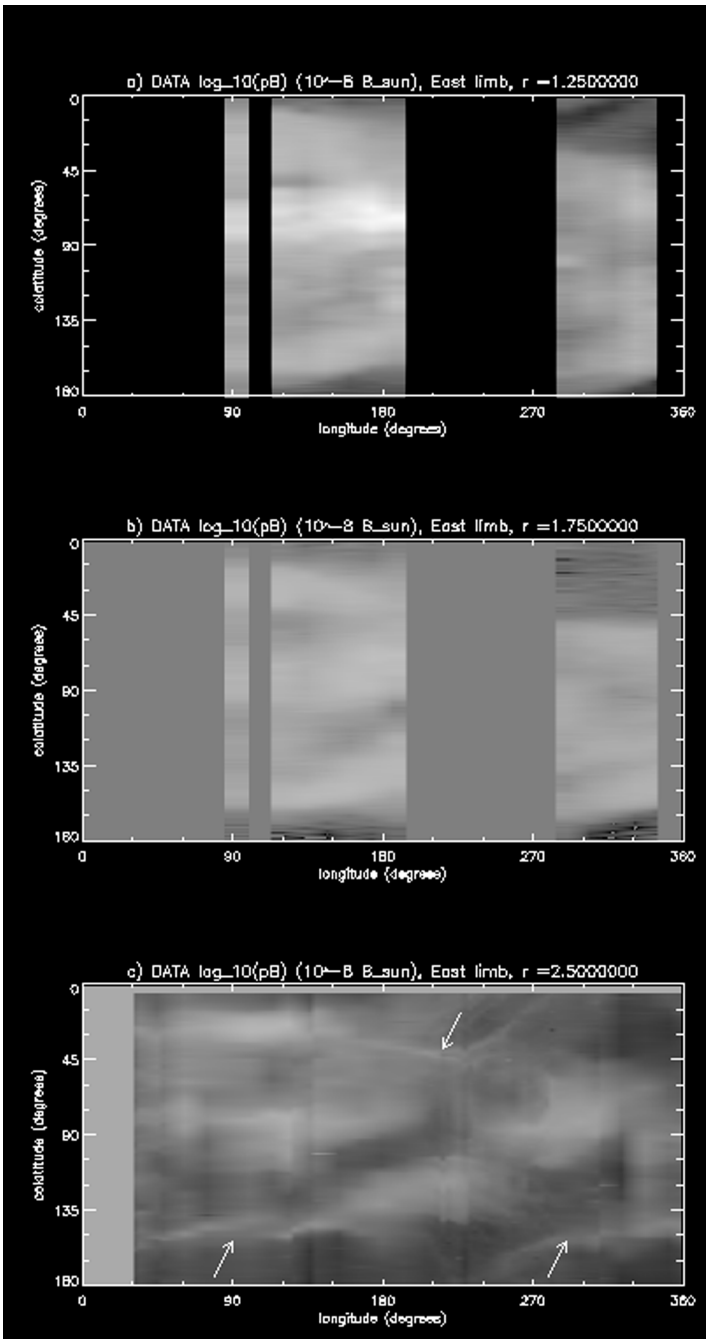

Figure 3. Carrington maps of a single solar rotation (CROT 1943, Nov/Dec 1998), showing observations of white light observable (pB) as a function of latitude vs. longitude, for three heights: $r = 1.25R_{sun}$; $r = 1.75R_{sun}$; and $r = 2.5R_{sun}$. Data are from the Mauna Loa Mark III K-Coronameter ($r = 1.25, 1.75R_{sun}$) and LASCO C2 Coronagraph ($r = 2.5R_{sun}$). Missing data due to weather for the Mark III instrument appear as vertical black bands. Arrows point to "bananas" as described in the text.

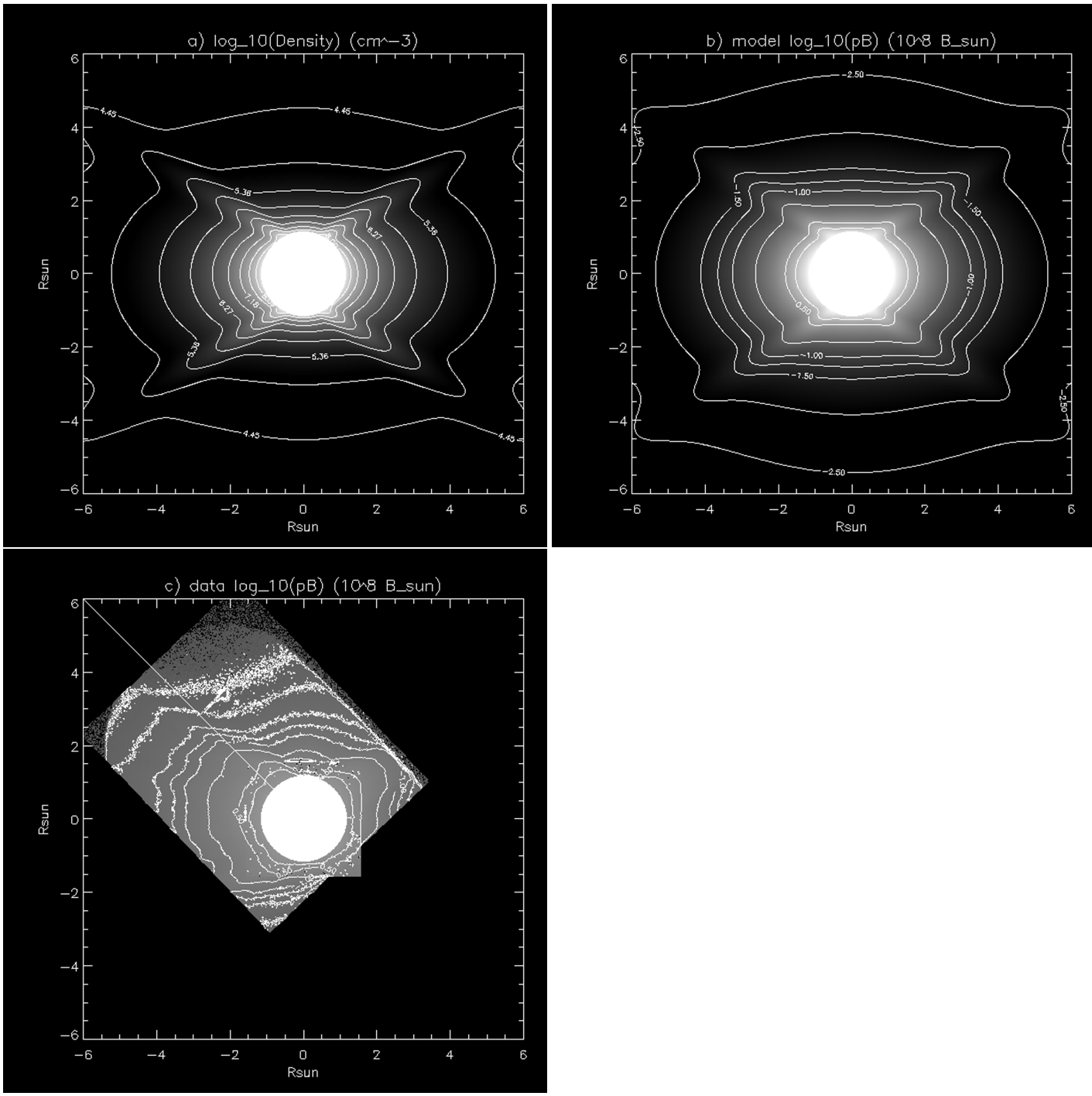

Figure 4. a) Axisymmetric density model demonstrating the incorporation of three streamer belts, and the nonradiality of the two high latitude belts; b) white light observable (pB) calculated from density model; c) composite image of observed pB from Spartan 201-05 White Light Coronagraph and Mauna Loa Mark III K-Coronameter data, November 1, 1998 (see *Gibson et al., 2003*).

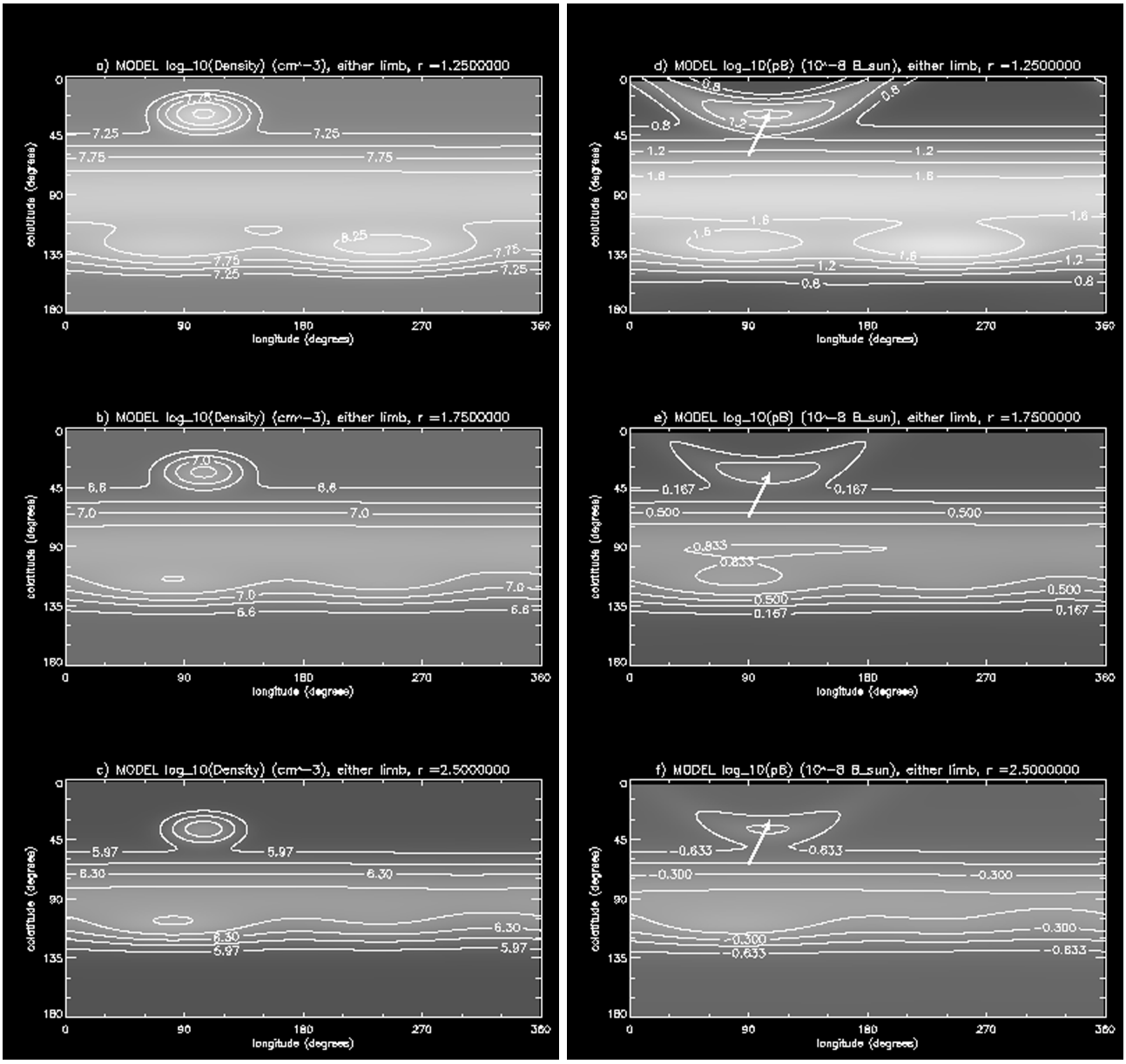

Figure 5. a-c) Carrington maps of a single hypothetical model solar rotation, latitude vs. longitude, showing a 3D density model that demonstrates the incorporation of four nonradial streamers having finite longitudinal length, for three radial heights a) $1.25R_{sun}$; b) $1.75R_{sun}$; and c) $2.5R_{sun}$; d-f) white light observable (pB) calculated from density model for same three heights.

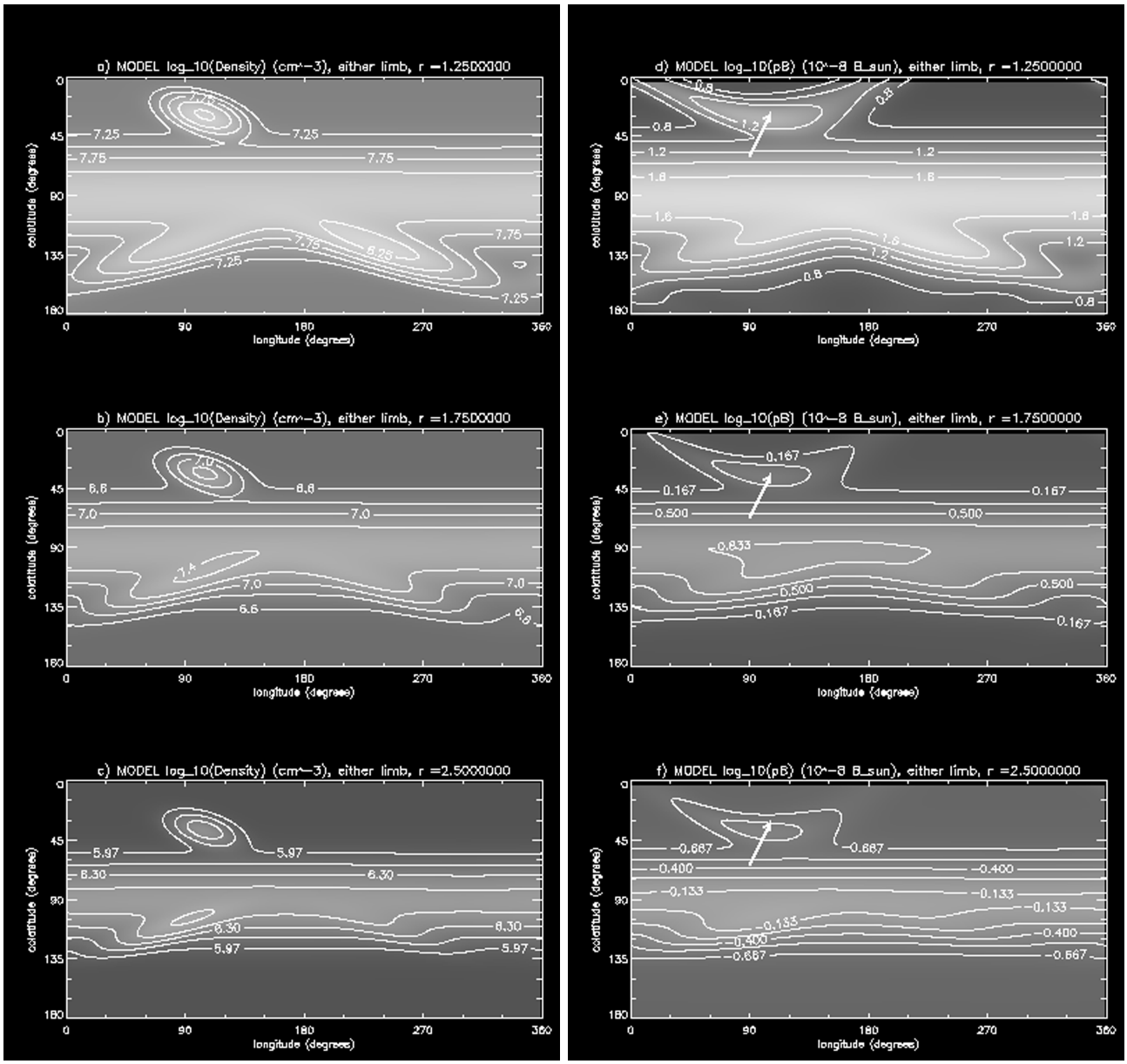

Figure 6. Carrington maps of a single solar hythothetical model rotation, latitude vs. longitude, showing a 3D density model that incorporates the same four streamers as Figure 3, except with underlying neutral lines that vary with both latitude and longitude. a-c) model density for three radial heights a) $1.25R_{sun}$; b) $1.75R_{sun}$; and c) $2.5R_{sun}$; d-f) white light observable (pB) calculated from density model for same three heights.

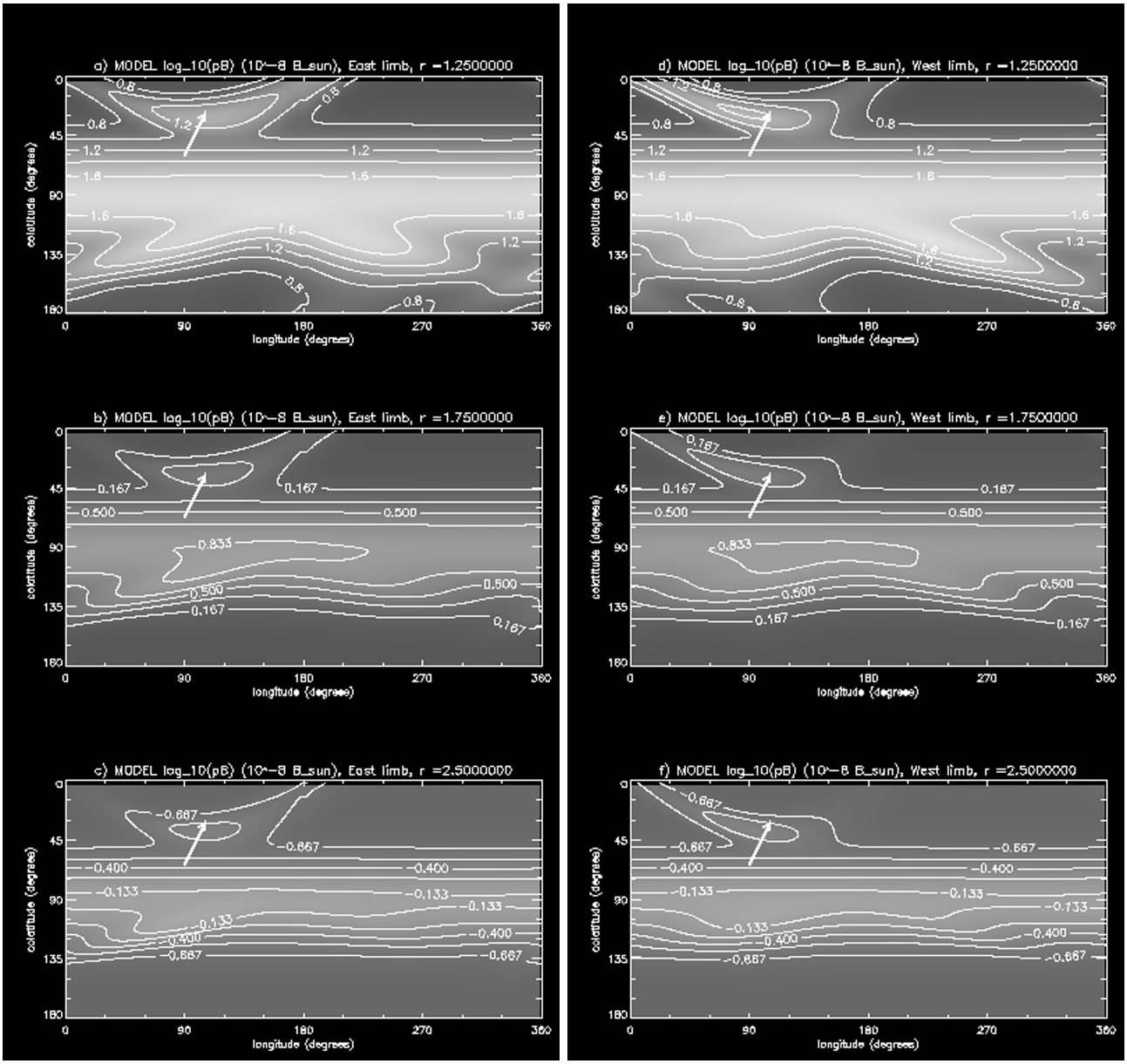

Figure 7. Carrington maps of pB for a single hypothetical model solar rotation, latitude vs. longituude, determined from a 3D density model that incorporates the same four streamers as Figure 4, except integrated along the line-of-sight for a maximal solar B angle equal to 7.25°. a-c) pB map for obervations from the East limb for three radial heights a) $1.25R_{sun}$; b) $1.75R_{sun}$; and c) $2.5R_{sun}$; d-f) pB Carrington map for West limb for same three heights.